Electronic Supplementary Material (ESI) for Dalton Transactions.
This journal is © The Royal Society of Chemistry 2022

*Supporting information*

# Self-assembly of Ni(II) metallacycles (a square and a triangle) supported by tetrazine-radical bridges

Te Wang, Binling Yao, Zhilin Guo, Xiaoyong Chang, Yi-Fei Deng,* and Yuan-Zhu Zhang*

Department of Chemistry, Southern University of Science and Technology (SUSTech), Shenzhen 518055, China.

**Table S1.** Selected bond lengths [Å] and angles [deg] for **1**.

| | | | |
|---|---|---|---|
| Ni1-N5 | 2.081(3) | Ni2-N2A | 2.002(3) |
| Ni1-N9A | 2.081(3) | Ni2-N8 | 2.112(3) |
| Ni1-N1A | 2.074(3) | Ni2-N8C | 2.112(3) |
| Ni1-N1 | 2.074(3) | N3-N4 | 1.395(4) |
| Ni1-N9A | 2.147(3) | N1-N2 | 1.372(3) |
| Ni1-N9 | 2.147(3) | N3-C6 | 1.310(4) |
| Ni2-N5A | 2.113(3) | N1-C6 | 1.324(4) |
| Ni2-N5B | 2.113(3) | N4-C7 | 1.313(4) |
| Ni2-N2 | 2.002(3) | N2-C7 | 1.334(4) |
| N5A-Ni1-N5 | 93.56(15) | N5B-Ni2-N5A | 97.36(15) |
| N5A-Ni1-N9 | 157.99(10) | N2-Ni2-N5B | 93.63(10) |
| N5-Ni1-N9 | 94.72(10) | N2C-Ni2-N5B | 86.86(10) |
| N1A-Ni1-N5 | 85.37(10) | N2C-Ni2-N2 | 179.27(15) |
| N1A-Ni1-N5A | 91.53(10) | N2-Ni2-N8 | 76.84(11) |
| N1-Ni1-N1A | 175.47(14) | N2C-Ni2-N8 | 102.62(11) |
| N1A-Ni1-N9A | 74.06(10) | N8C-Ni2-N5A | 90.41(11) |
| N9A-Ni1-N1 | 109.43(10) | N8-Ni2-N5A | 162.37(10) |
| N9A-Ni1-N9 | 85.06(14) | N8C-Ni2-N8 | 86.71(16) |

Symmetry transformations used to generate equivalent atoms:

A: 1/4+y, -1/4+x, 3/4-z; B: 3/4-y, 3/4-x, 3/4-z; C: 1-x, 1/2-y, +z.

**Table S2.** Selected bond lengths [Å] and angles [deg] for **2**.

| | | | |
|---|---|---|---|
| Ni1-N4A | 2.069(3) | N1-N2 | 1.379(4) |
| Ni1-N12 | 2.127(3) | N3-N4 | 1.384(4) |
| Ni1-N11A | 2.152(3) | N1-C10 | 1.340(3) |
| Ni1-N1 | 2.028(3) | N3-C10 | 1.316(5) |
| Ni1-N9 | 2.140(3) | N4-C11 | 1.324(5) |
| Ni1-N5 | 2.043(3) | N2-C11 | 1.318(5) |
| N5-N6 | 1.391(5) | N7-C30 | 1.302(6) |
| N7-N8 | 1.396(6) | N6-C31 | 1.323(5) |
| N5-C30 | 1.333(5) | N8-C31 | 1.311(6) |
| N4A-Ni1-N12 | 88.87(12) | N1-Ni1-N9 | 172.87(13) |
| N4A-Ni1-N11A | 77.63(12) | N1-Ni1-N5 | 100.08(14) |
| N4A-Ni1-N9 | 96.16(14) | N9-Ni1-N11A | 82.12(13) |
| N12-Ni1-N11A | 163.54(13) | N5-Ni1-N4A | 170.81(13) |
| N12-Ni1-N9 | 108.97(13) | N5-Ni1-N12 | 98.37(12) |
| N1-Ni1-N4A | 86.97(13) | N5-Ni1-N11A | 96.07(12) |
| N1-Ni1-N12 | 77.42(12) | N5-Ni1-N9 | 76.18(15) |
| N1-Ni1-N11A | 92.33(13) | | |

Symmetry transformations used to generate equivalent atoms:

A: 1-y, +x-y, +z; B: 1+y-x, 1-x, +z;

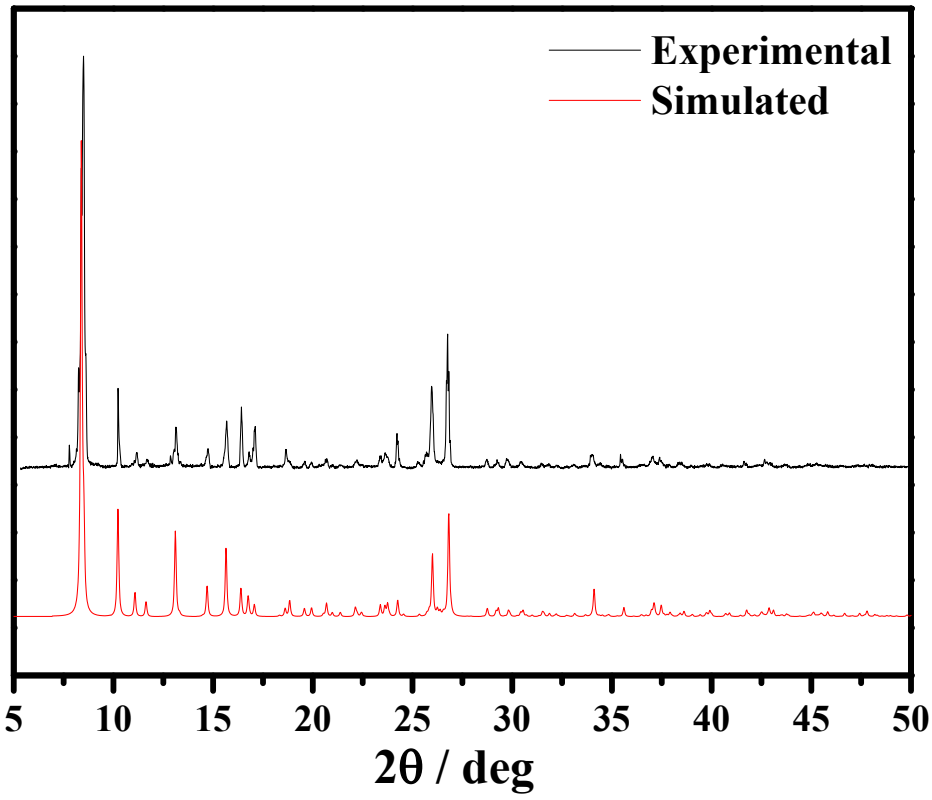


**Fig. S1** Powder X-ray diffraction pattern and the simulation from the single crystal data of **1**.

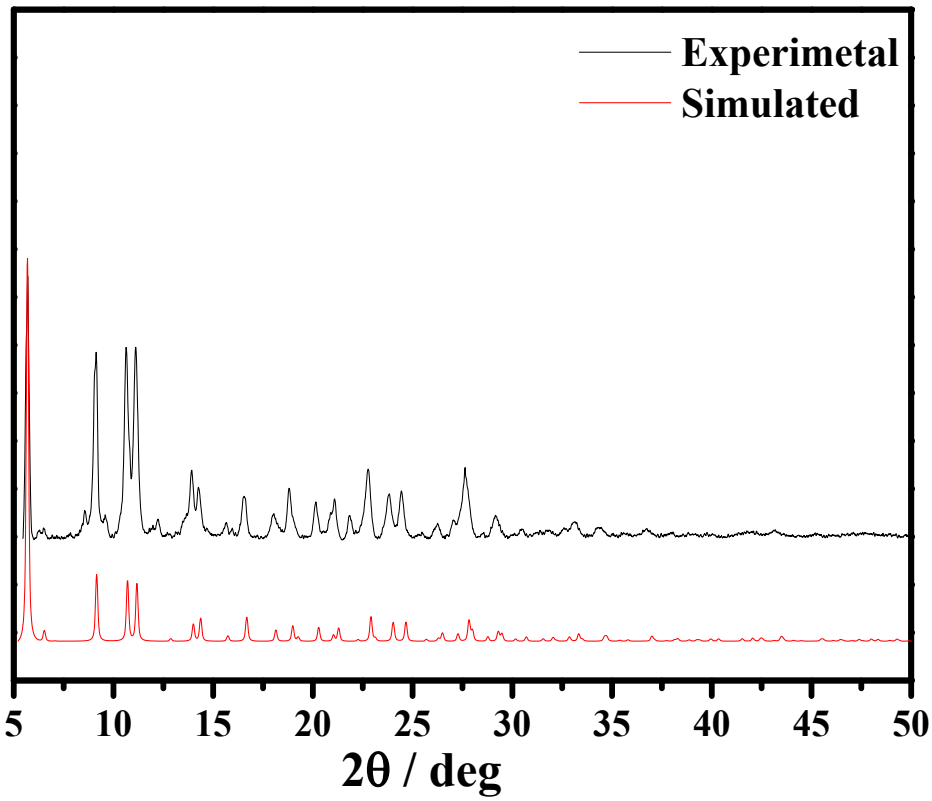


**Fig. S2** Powder X-ray diffraction pattern and the simulation from the single crystal data of **2**.

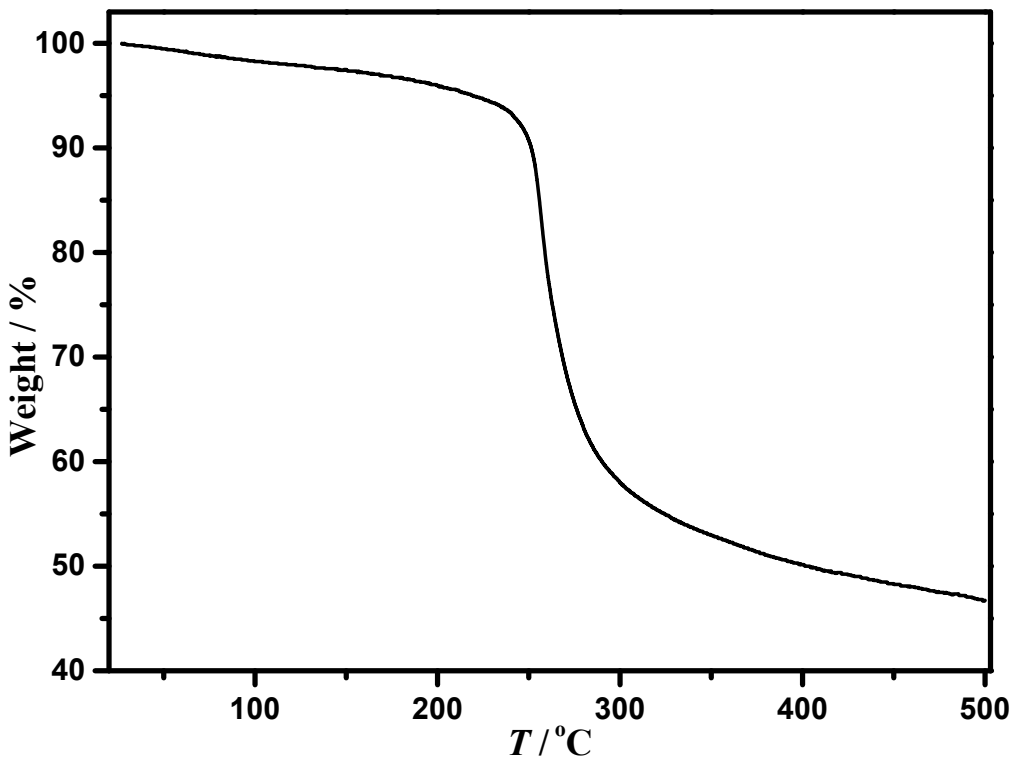


**Fig. S3** TGA curve of **1** at a rate of 10 K/min under an argon atmosphere.

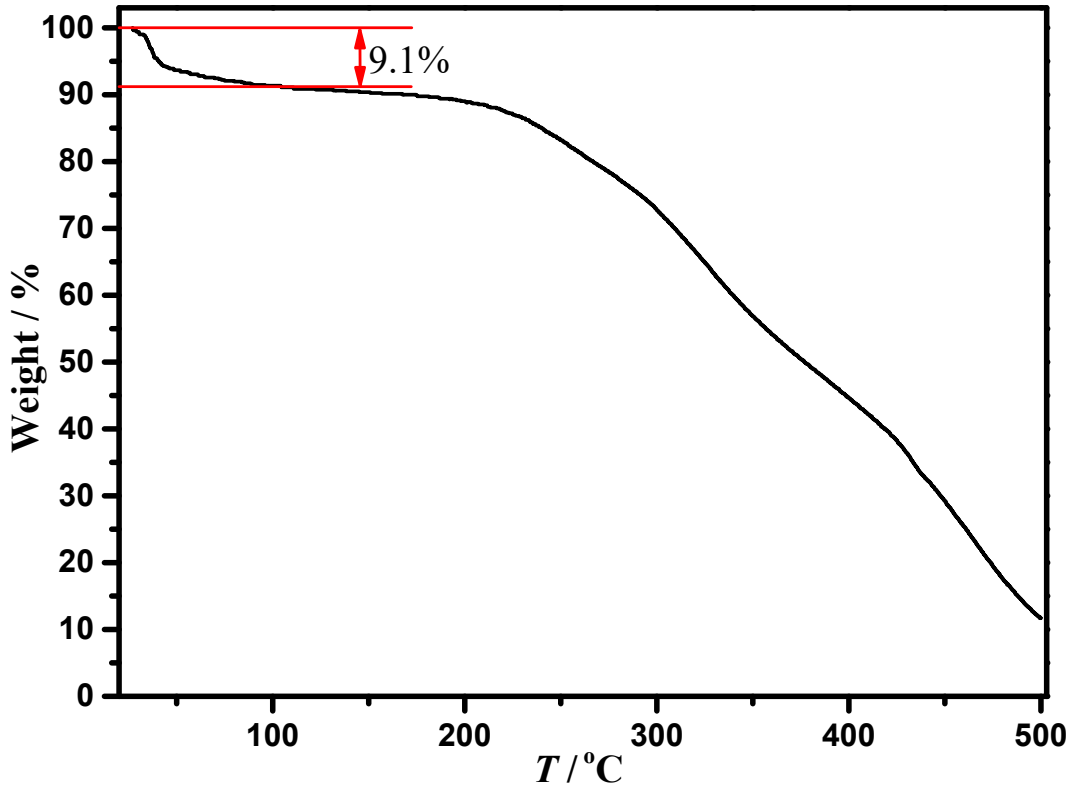


**Fig. S4** TGA curve of **2** at a rate of 10 K/min under an argon atmosphere.

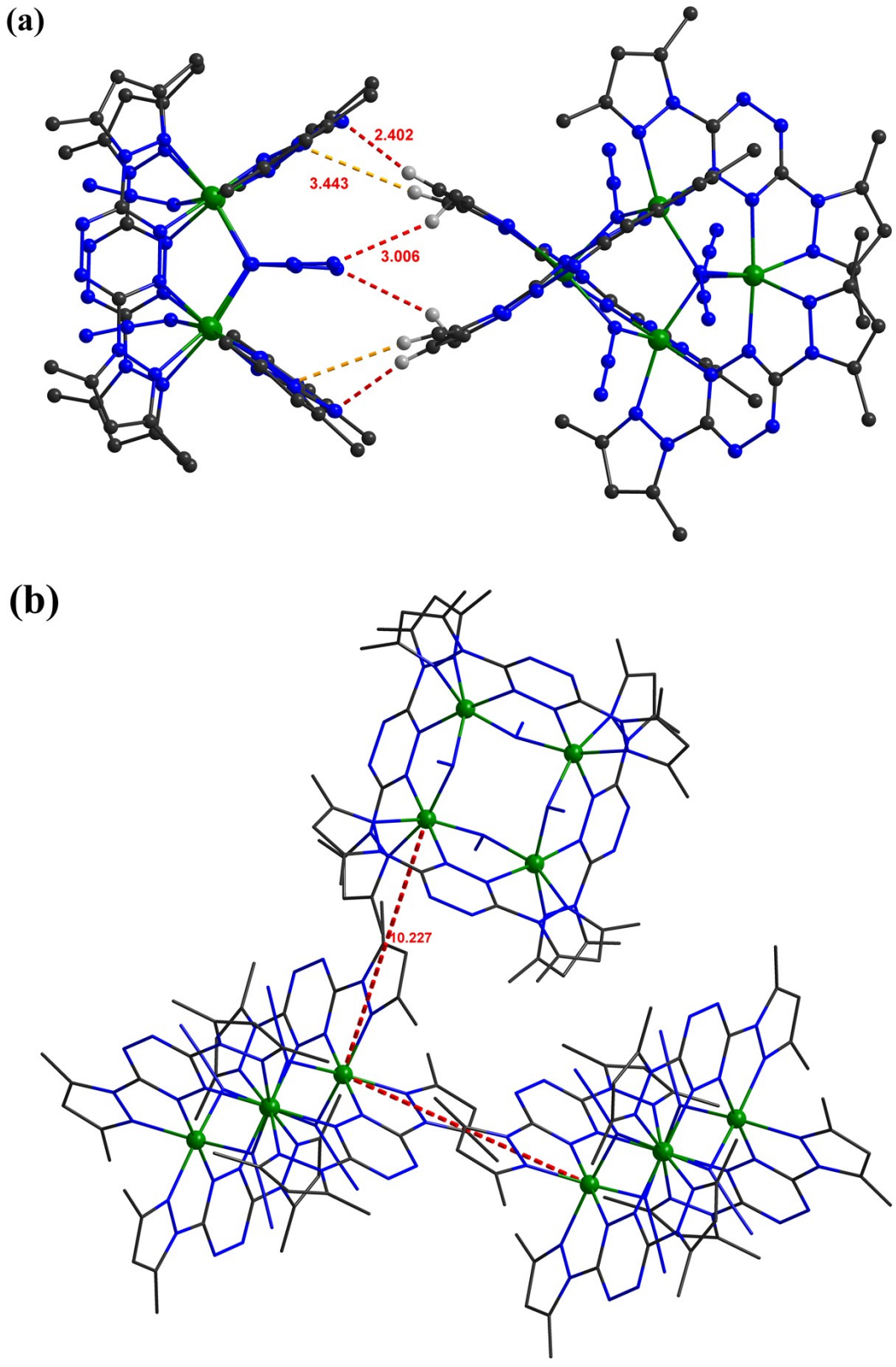


**Fig. S5** The packing diagram (a) of **1** illustrating the short contacts around the neighbouring squares. The red and yellow dashed lines represent the N···H hydrogen bonds (2.402, 3.006 Å) and C-H···π (3.443 Å) couplings, respectively. Fig. S5b shows the nearest intercluster Ni···Ni distance (10.227 Å). Ni(II), green; C, dark grey; N, blue; H, pale grey. Other hydrogen atoms are omitted for clarity.

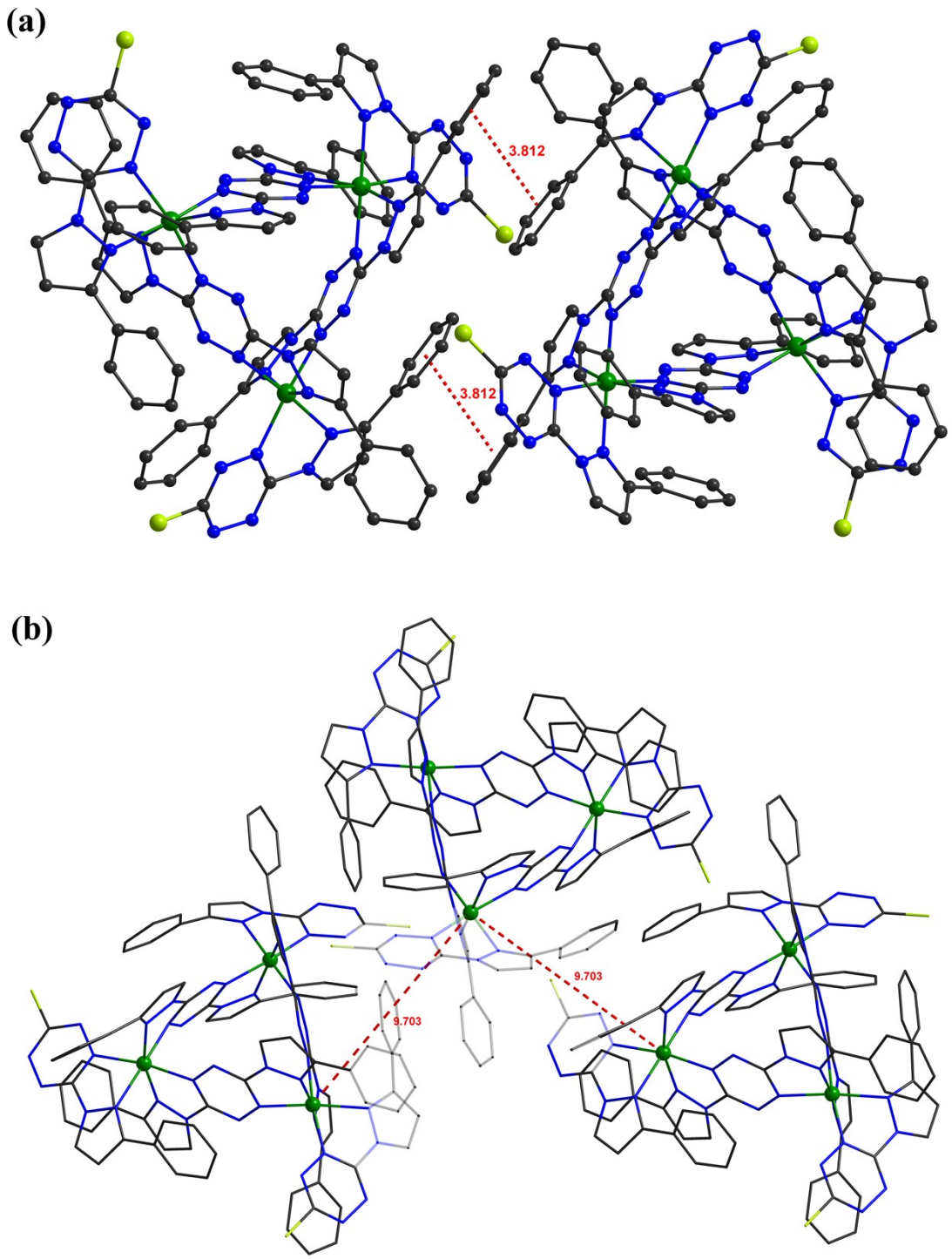


**Fig. S6** The packing diagram (a) of **2** showing the π···π interactions (red dashed line, 3.812 Å) between the neighbouring triangles. Fig. S6b gives the nearest intercluster Ni···Ni distance (9.703 Å). Ni(II), green; C, dark grey; Cl, lime; N, blue. Hydrogen atoms and lattice solvent molecules are omitted for clarity.

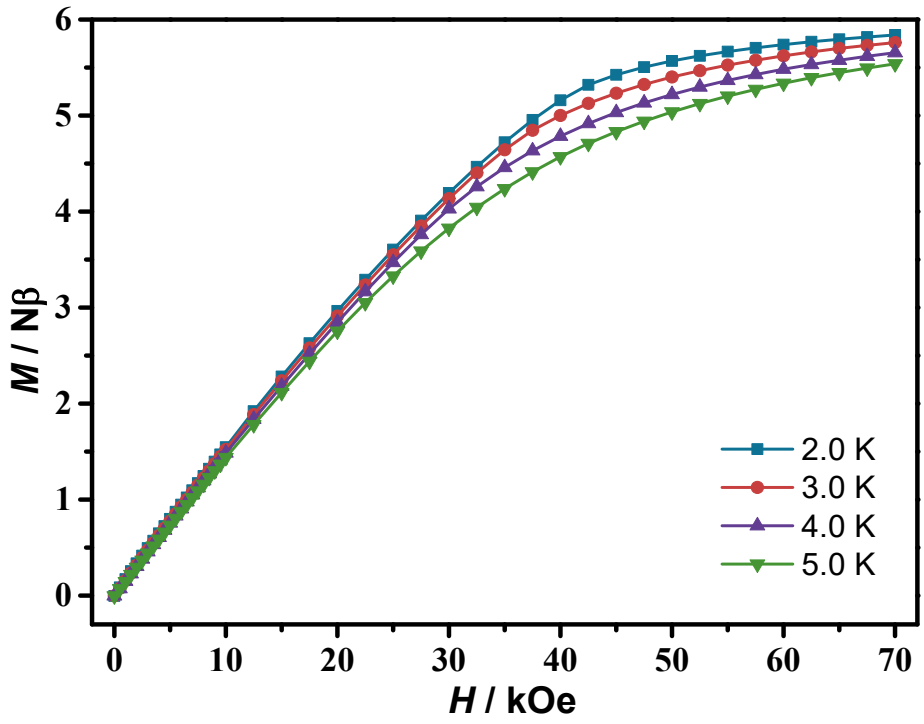


**Fig. S7** Field-dependent magnetization data for **1** at 2-5 K. Solid lines are guides for the eye.

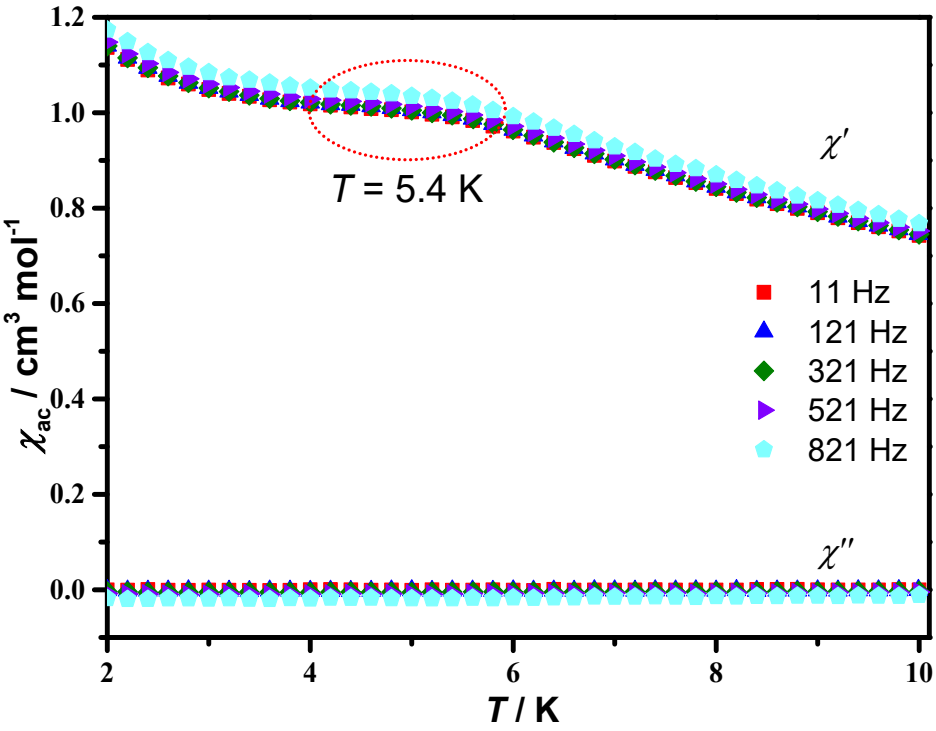


**Fig. S8** Temperature dependence of the in-phase ($\chi'$) and out-of-phase ($\chi''$) ac magnetic susceptibilities for **1** under zero dc field.

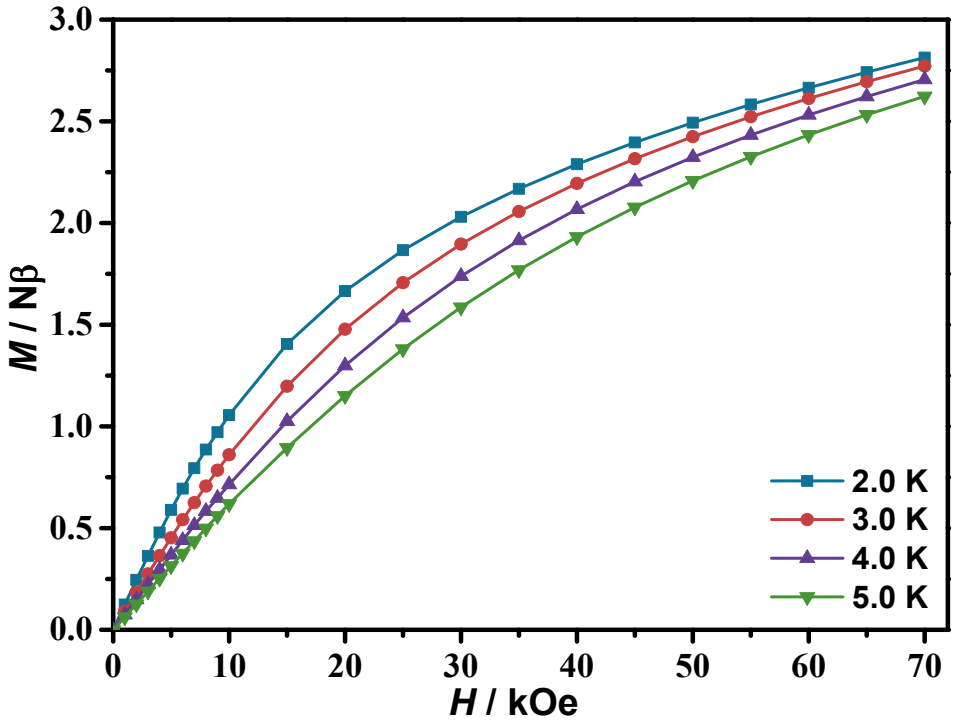


**Fig. S9** Field-dependent magnetization data for **2** at 2-5 K. Solid lines are guides for the eye.

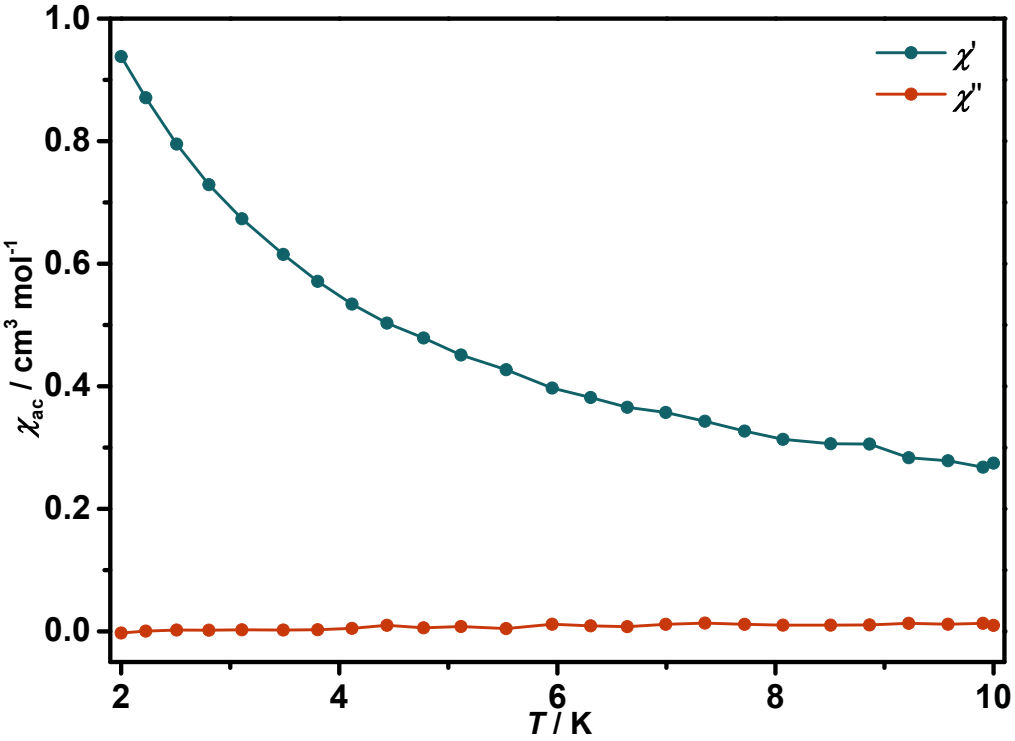


**Fig. S10** Temperature dependence of the in-phase ($\chi'$) and out-of-phase ($\chi''$) ac magnetic susceptibilities for **2** under zero dc field (972 Hz). Solid lines are guides for the eye.

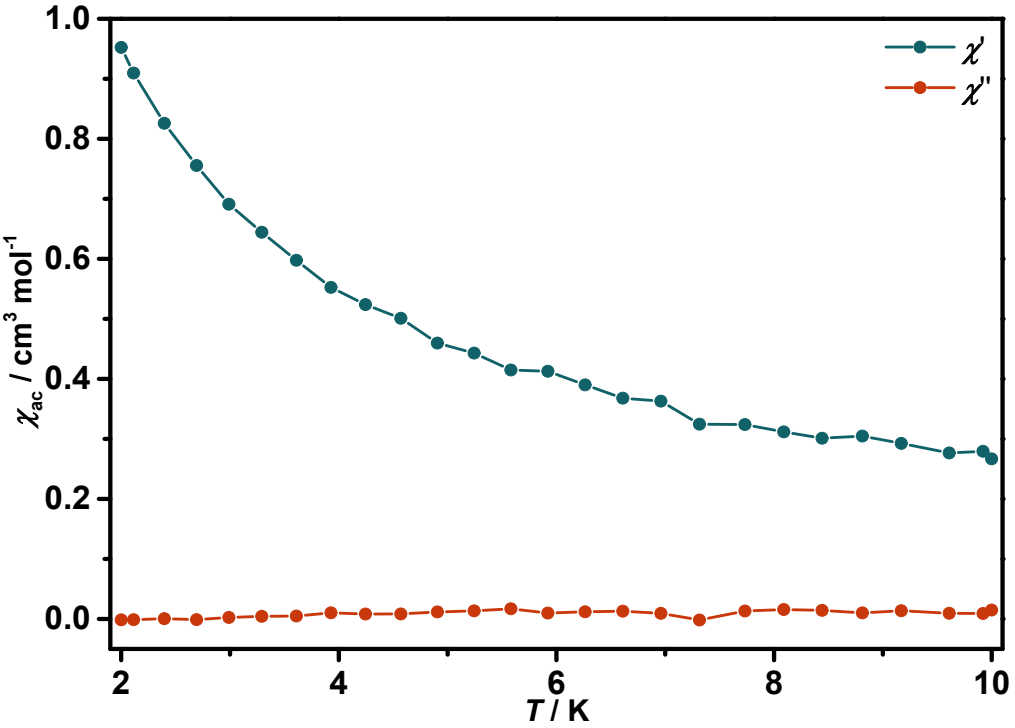


**Fig. S11** Temperature dependence of the in-phase (χ′) and out-of-phase (χ′′) ac magnetic susceptibilities for **2** under 1000 Oe dc field (972 Hz). Solid lines are guides for the eye.

The detailed magnetic fittings were carried out by adding the variables incrementally via 8 spin models. To avoid the over-parameterization, $g_{Ni}$ and $g_{rad}$ values were fixed as 2.2 and 2.0 respectively according to those of **1**, and the interactions between the radicals (either the terminal or the bridging ones) were restricted as the same. The magnetic data were fitted using the PHI program according to the following Hamiltonians, where $\mu_B$ is the Bohr magneton; H is the magnetic field vector; $g_{Ni}$ and $g_{rad}$ are the Lande factors for Ni(II) ion and tetrazine radical, respectively; $D_{Ni}$ corresponds to the axial zero-field splitting (zfs) parameter; $S_1$ to $S_3$ = 1 for $Ni^{2+}$; $S_A$ to $S_F$ = 1/2 for the tetrazine radicals; $J_1$, $J_2$, $J_3$ $J_4$ and *zj′* correspond to the Ni-$rad_{bridging}$, Ni-$rad_{terminal}$, Ni-Ni, rad-rad and intermolecular couplings, respectively.

1. Ni-$rad_{bridging}$ ($J_1$) and Ni-$rad_{terminal}$ ($J_2$) couplings are included.

$$H = -2J_1(\hat{S}_1\hat{S}_B + \hat{S}_B\hat{S}_2 + \hat{S}_2\hat{S}_D + \hat{S}_D\hat{S}_3 + \hat{S}_3\hat{S}_F + \hat{S}_F\hat{S}_1) - 2J_2(\hat{S}_1\hat{S}_A + \hat{S}_2\hat{S}_C + \hat{S}$$

)

**Model A**: without intermolecular coupling (*zj′*); **Model B**: with intermolecular coupling (*zj′*).

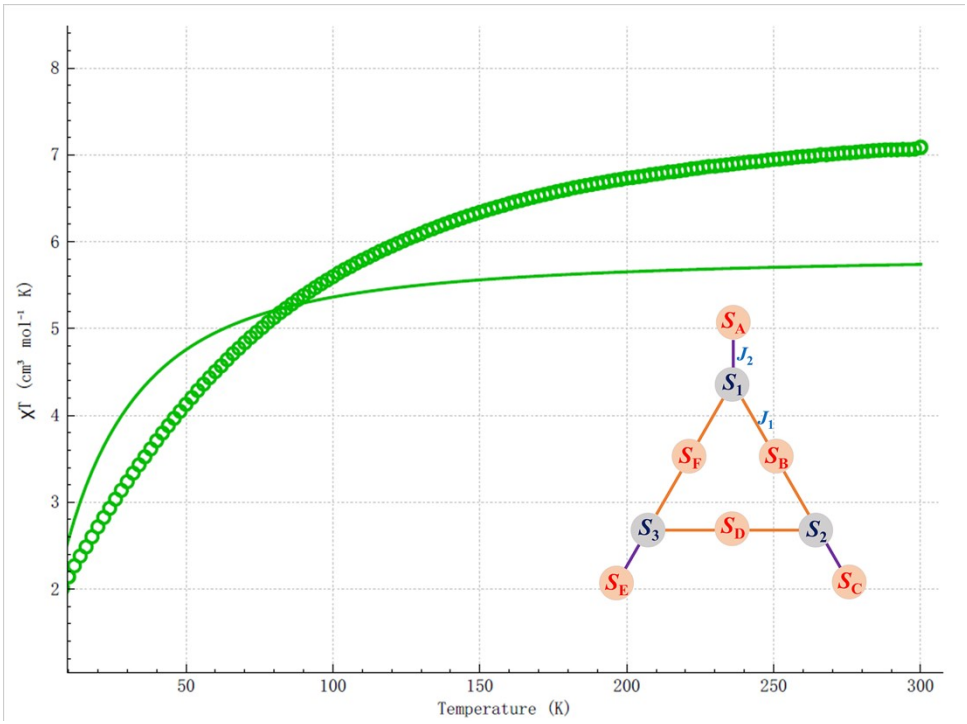


**Fig. S12** Experimental magnetic susceptibility at 1000 Oe dc for **2** along with its fit based on model A. Inset shows the magnetic exchange pathways.

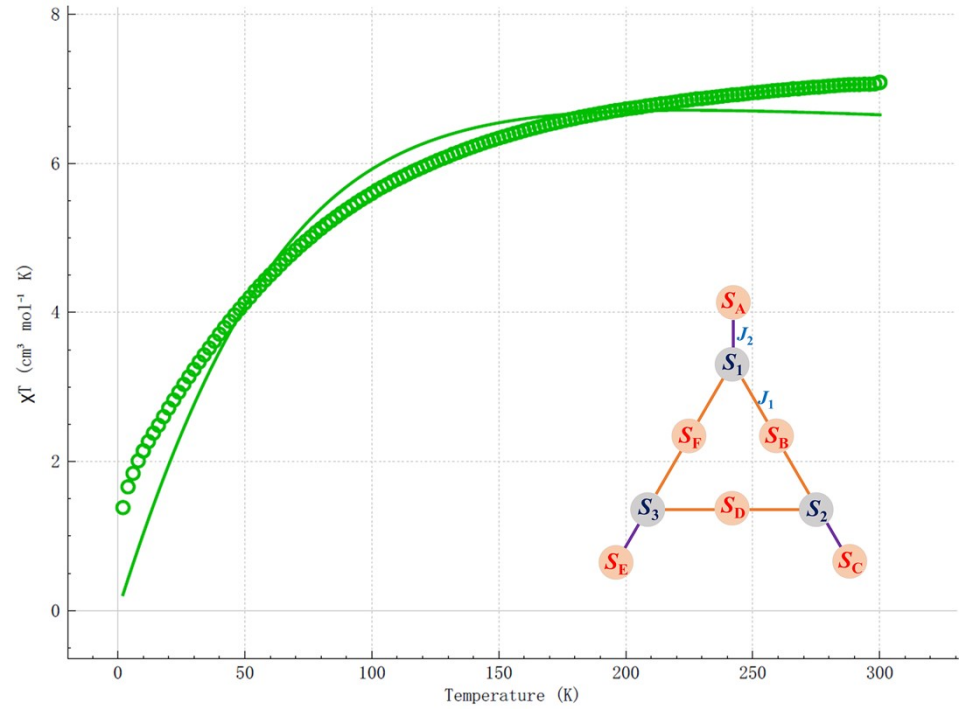


**Fig. S13** Experimental magnetic susceptibility at 1000 Oe dc for **2** along with its fit based on model B. Inset shows the magnetic exchange pathways.

2. Ni-rad$_{bridging}$ ($J_1$), Ni-rad$_{terminal}$ ($J_2$) and Ni-Ni ($J_3$) couplings are included.

$$H = -2J_1(\hat{S}_1\hat{S}_B + \hat{S}_B\hat{S}_2 + \hat{S}_2\hat{S}_D + \hat{S}_D\hat{S}_3 + \hat{S}_3\hat{S}_F + \hat{S}_F\hat{S}_1) - 2J_2(\hat{S}_1\hat{S}_A + \hat{S}_2\hat{S}_C + \hat{S}_3\hat{S}_E)$$
$$-2J_3(\hat{S}_1\hat{S}_2 + \hat{S}_2\hat{S}_3 + \hat{S}_3\hat{S}_1) + \sum_{i=A}^{F} g_{rad}\mu_B\hat{S}_i H + \sum_{i=1}^{3}(D_{Ni,i}\hat{S}_{z,i}^2 + g_{Ni}\mu_B\hat{S}_i H)$$

**Model C**: without intermolecular coupling (*zj'*); **Model D**: with intermolecular coupling (*zj'*).

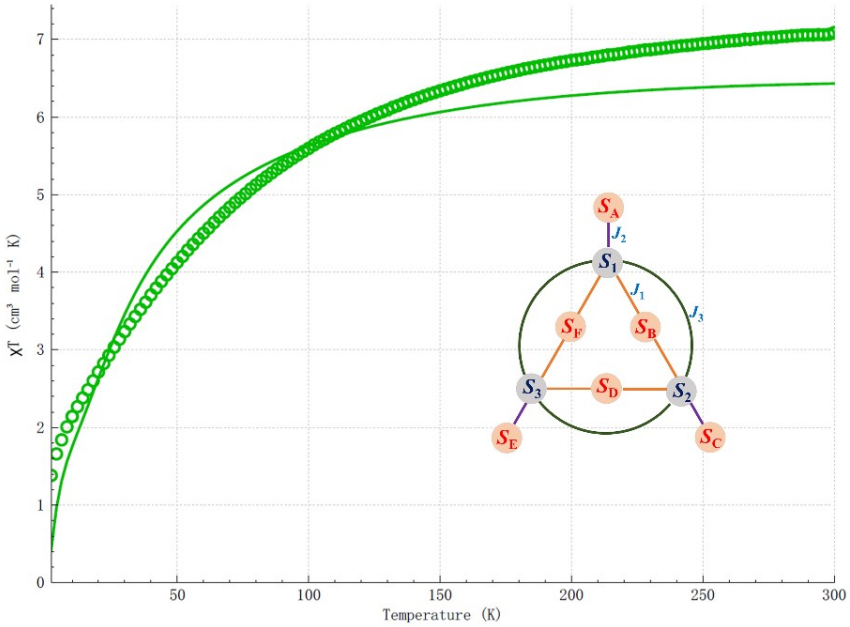


**Fig. S14** Experimental magnetic susceptibility at 1000 Oe dc for **2** along with its fit based on model C. Inset shows the magnetic exchange pathways.

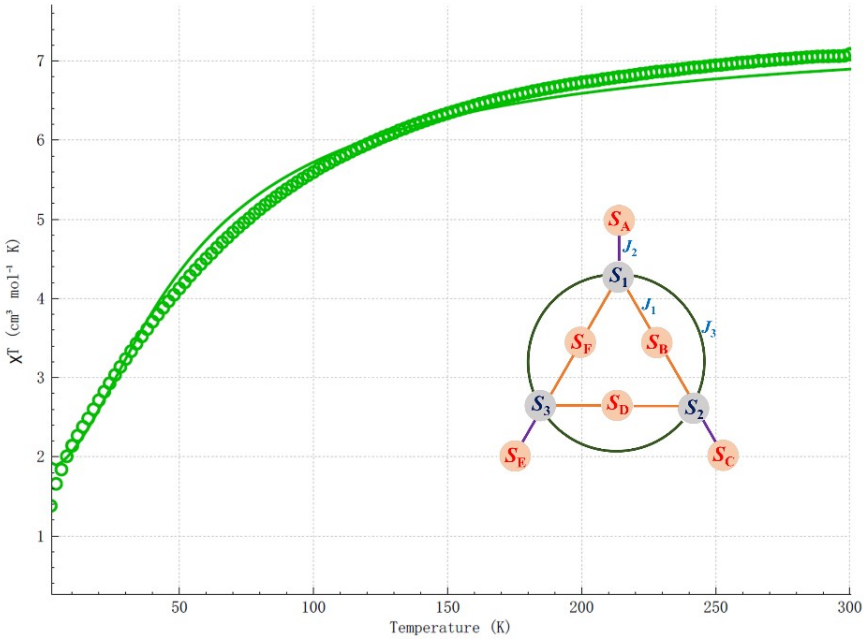


**Fig. S15** Experimental magnetic susceptibility at 1000 Oe dc for **2** along with its fit based on model D. Inset shows the magnetic exchange pathways.

3. Ni-rad$_{bridging}$ ($J_1$), Ni-rad$_{terminal}$ ($J_2$) and rad-rad ($J_4$) couplings are included.

$$H = -2J_1(\hat{S}_1\hat{S}_B + \hat{S}_B\hat{S}_2 + \hat{S}_2\hat{S}_D + \hat{S}_D\hat{S}_3 + \hat{S}_3\hat{S}_F + \hat{S}_F\hat{S}_1) - 2J_2(\hat{S}_1\hat{S}_A + \hat{S}_2\hat{S}_C + \hat{S}$$
$$+ \sum_{i=A}^{F} g_{rad}\mu_B\hat{S}_i H + \sum_{i=1}^{3}(D_{Ni,i}\hat{S}_{z,i}^2 + g_{Ni}\mu_B\hat{S}_i H)$$

**Model E**: without intermolecular coupling (*zj'*); **Model F**: with intermolecular coupling (*zj'*).

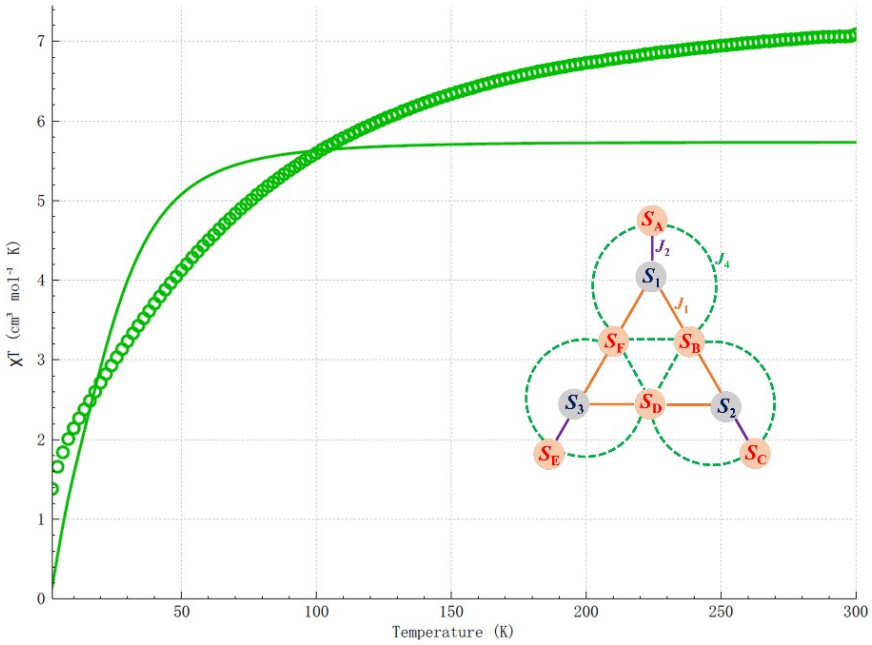


**Fig. S16** Experimental magnetic susceptibility at 1000 Oe dc for **2** along with its fit based on model E. Inset shows the magnetic exchange pathways.

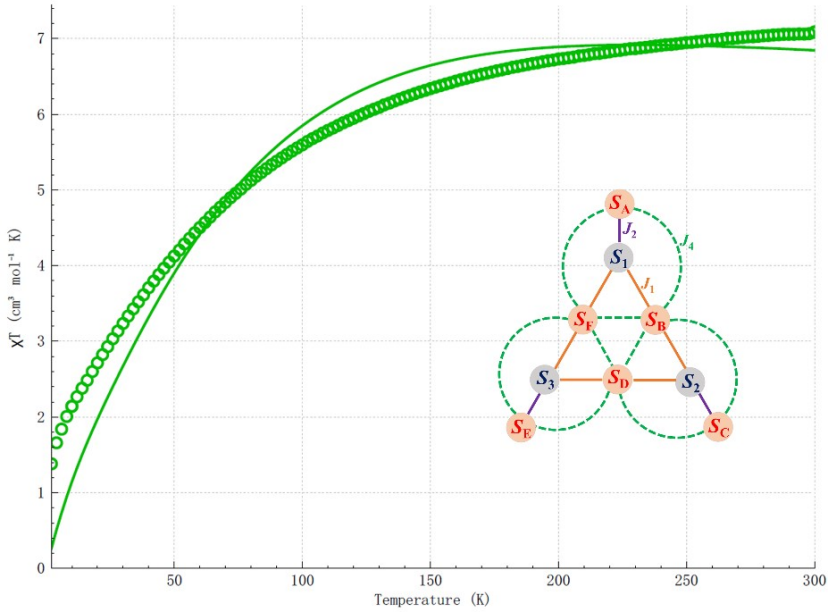

**Fig. S17** Experimental magnetic susceptibility at 1000 Oe dc for **2** along with its fit based on model F. Inset shows the magnetic exchange pathways.

4. Ni-rad$_{bridging}$ ($J_1$), Ni-rad$_{terminal}$ ($J_2$), Ni-Ni ($J_3$) and rad-rad ($J_4$) couplings are included.

$$H = -2J_1(\hat{S}_1\hat{S}_B + \hat{S}_B\hat{S}_2 + \hat{S}_2\hat{S}_D + \hat{S}_D\hat{S}_3 + \hat{S}_3\hat{S}_F + \hat{S}_F\hat{S}_1) - 2J_2(\hat{S}_1\hat{S}_A + \hat{S}_2\hat{S}_C + \hat{S}_3\hat{S}_E) - 2J_3(\hat{S}_1\hat{S}_2$$
$$+ \sum_{i=A}^{F} g_{rad}\mu_B\hat{S}_i H + \sum_{i=1}^{3}(D_{Ni,i}\hat{S}_{z,i}^2 + g_{Ni}\mu_B\hat{S}_i H)$$

**Model G**: without intermolecular coupling (*zj'*); **Model H**: with intermolecular coupling (*zj'*).

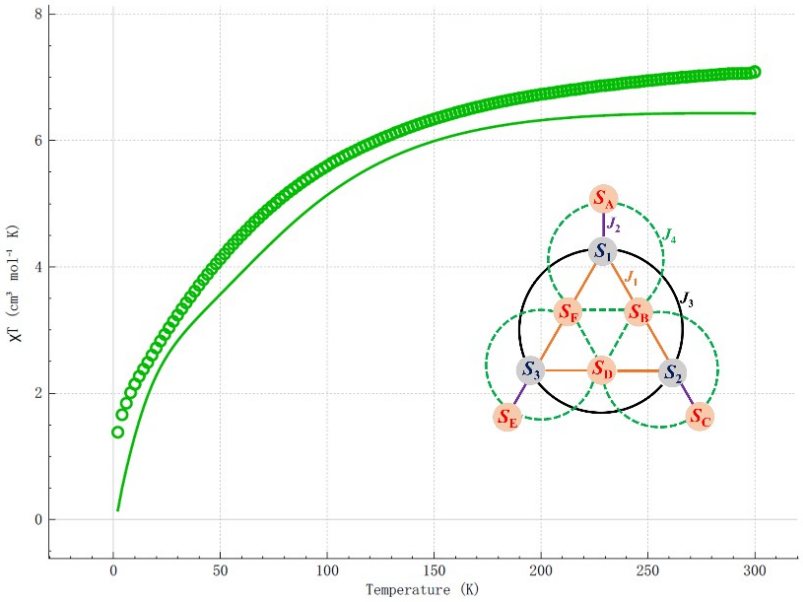


**Fig. S18** Experimental magnetic susceptibility at 1000 Oe dc for **2** along with its fit based on model G. Inset shows the magnetic exchange pathways.

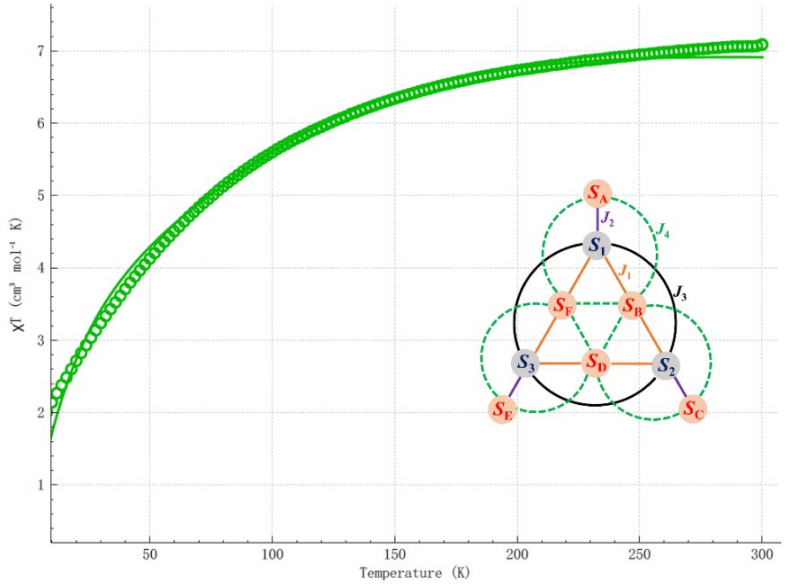


**Fig. S19** Experimental magnetic susceptibility at 1000 Oe dc for **2** along with its fit based on model H. Inset shows the magnetic exchange pathways.

The magnetic susceptibility data were fitted based on models A-H (Figs. S12-19), and the best set of parameters are summarized in Table S3. As we can see, no acceptable fits could be obtained based on models A, B, C, E, F and G. For model D, the fitted $\chi_M T$ vs $T$ plots matched well with those experimentally determined while the obtained parameters, especially for $J_1$ and $J_2$ significantly deviated from the literature reports for similar tetrazine-radical bridged Ni(II) systems. For model H, the magnetic susceptibility data were well reproduced, and the obtained coupling constants and zfs parameters were in agreement with those reported Ni(II) complex bearing the similar tetrazine-radical bridging ligands or coordination models. These results could reasonably demonstrate the necessity of each parameter for the magnetic fitting of **2**.

**Table S3**. The best-fit parameters based on the spin models A-H.

| Model | $D_{Ni}$ ($cm^{-1}$) | $J_1$ ($cm^{-1}$) | $J_2$ ($cm^{-1}$) | $J_3$ ($cm^{-1}$) | $J_4$ ($cm^{-1}$) | $zj'$ ($cm^{-1}$) | $R$ ($\sum(\chi_0-\chi_c)^2/\sum\chi_o^2$) |
|---|---|---|---|---|---|---|---|
| A | -5.34 | -0.56 | -8.24 | | | | 0.0298 |
| B | 9.14 | 71.9 | 12.62 | | | -2.42 | 0.0042 |
| C | 2.28 | 158.54 | -3 | -60.68 | | | 0.0049 |
| D | 26.66 | 11.53 | 513 | -6.09 | | -0.32 | 0.0027 |
| E | 2.56 | -0.18 | -14.81 | | 16.28 | | 0.0227 |
| F | -1.89 | 72.99 | -53.72 | | 43.29 | -1.89 | 0.0036 |
| G | -0.45 | 3.71 | -54.9 | 35.48 | 22.39 | | 0.0076 |
| H | 3.1 | 95.4 | -57.5 | 0.6 | -0.3 | -0.8 | 0.0012 |